Southern Ocean Response to Strengthening Winds in an Eddy-Permitting Global Climate Model

PAUL SPENCE

Climate Change Research Centre, University of New South Wales, Sydney, New South Wales, Australia

JOHN C. FYFE

Canadian Centre for Climate Modelling and Analysis, Environment Canada, University of Victoria, Victoria, British Columbia, Canada

ALVARO MONTENEGRO AND ANDREW J. WEAVER

School of Earth and Ocean Science, University of Victoria, Victoria, British Columbia, Canada

(Manuscript received 20 February 2009, in final form 8 April 2010)

ABSTRACT

A global climate model with horizontal resolutions in the ocean ranging from relatively coarse to eddy permitting is used to investigate the resolution dependence of the Southern Ocean response to poleward intensifying winds through the past and present centuries. The higher-resolution simulations show poleward migration of distinct ocean fronts associated with a more highly localized near-surface temperature response than in the lower-resolution simulations. The higher-resolution simulations also show increasing southward eddy heat transport, less high-latitude cooling, and greater sea ice loss than the lower-resolution simulations. For all resolutions, from relatively coarse to eddy permitting, there is poleward migration of the Antarctic Circumpolar Current in the Atlantic and the western half of the Indian basin. Finally, zonal transports associated with the Antarctic Circumpolar Current are shown to be sensitive to resolution, and this is discussed in the context of recent observed change.

1. Introduction

Observations from the past few decades indicate that a section of the Southern Ocean between 40° and 60°S has been warming at nearly twice the rate of the global ocean (Gille 2002; Aoki et al. 2003; Gille 2008). Concurrent atmospheric observations reveal a poleward shift and strengthening of Southern Hemisphere westerly winds, identified as a shift in the Southern Annual Mode (SAM) toward a higher index state (Thompson and Solomon 2002). The change in the southern winds appears to be due to anthropogenic forcing, with increasing atmospheric concentrations of both ozone-depleting gases (Gillett and Thompson 2003) and greenhouse gases (Fyfe 2006) identified as playing critical roles. Global climate models are remarkably consistent in simulating poleward intensifying surface winds through the past and present centuries (Fyfe and Saenko 2006). While Southern Ocean sea surface temperatures (SSTs) and the Antarctic Circumpolar Current (ACC) are observed to respond to SAM variability on interannual and seasonal time scales (Hughes et al. 2003; Ciasto and Thompson 2008), the effect of a longer-term anthropogenic SAM trend on the Southern Ocean is less certain. In particular, debate currently surrounds the ability of the relatively coarse-resolution GCMs (e.g., as analyzed in Fyfe and Saenko 2006) to accurately capture the Southern Ocean response to poleward intensifying winds (Meredith and Hogg 2006; Böning et al. 2008).

The oceanic temperature response in relatively coarse-resolution GCMs to poleward intensifying winds is a warming of surface to middepth waters along the northern edge of the ACC and a cooling at higher and lower latitudes (Sen Gupta and England 2006; Fyfe et al. 2007). This response is primarily due to an enhanced northward

Corresponding author address: Paul Spence, SEOS, University of Victoria, 3800 Finnerty Road, P.O. Box 3065, STN CSC, Victoria, BC V8W 3V6, Canada.
E-mail: paul.spence@ccrc.unsw.edu.au

DOI: 10.1175/2010JCLI3098.1

Ekman transport and changes in Ekman pumping. Relatively coarse-resolution models also show an increase in ACC transport that nearly linearly follows the maximum wind stress, as well as a poleward shift in its mean position (Fyfe and Saenko 2006). However, several factors have put into question the applicability to the real ocean of results from coarse-resolution GCMs that rely on parameterization schemes to indirectly account for the effects of mesoscale motion. It has been suggested that the ACC exists in an eddy saturated state wherein increasing mesoscale eddy fluxes transfer momentum and buoyancy in a manner opposing the direct wind-driven acceleration of the mean ACC seen in relatively coarse-resolution GCMs (Hallberg and Gnanadesikan 2001; Meredith and Hogg 2006; Böning et al. 2008). An enhanced meridional mesoscale eddy heat flux could significantly contribute to Southern Ocean warming (Hogg et al. 2008), as could the poleward displacement of finely structured Southern Ocean fronts (Gille 2008).

Unfortunately, current ocean eddy-resolving model studies are limited by computational constraints often requiring nonglobal spatial domains with idealized boundary conditions and short integration periods that subject model fields to extensive drifts. Regional eddy-resolving models have demonstrated that an increase in Southern Ocean wind stress tends to increase eddy kinetic energy and the poleward heat flux with little effect on the mean ACC transport (Hallberg and Gnanadesikan 2006; Meredith and Hogg 2006; Screen et al. 2009). However, as yet no ocean eddy-resolving climate model has been able to fully address the long-term anthropogenic response of the Southern Ocean to poleward intensifying winds through the twenty-first century.

This study aims to explore the gap between coarse and eddy-resolving GCMs. A global climate model is run over a range of horizontal resolutions to investigate the resolution dependence of the Southern Ocean response to poleward intensifying winds over the past and present century. Two sets of experiments investigating changes in Southern Ocean temperature, sea ice thickness, meridional ocean eddy heat transport, and the ACC are conducted. First, four model versions, ranging in horizontal resolution from 1.8° (latitude) × 3.6° (longitude) to 0.2° × 0.4°, are subject to poleward intensifying wind forcing from the year 1900 to 2100. Second, we evaluate the sensitivity of the highest-resolution model response to an increase in resolved mesoscale activity. In this experiment, both a high– and low–horizontal viscosity 0.2° × 0.4° model are forced from their year 1900 control state with predicted wind anomalies from 2060 to 2100.

2. Methods

The University of Victoria Earth System Climate Model (UVic ESCM) couples a vertically integrated energy–moisture balance atmospheric model, a thermodynamic/dynamic sea ice model, and a land surface model with the Geophysical Fluid Dynamics Laboratory (GFDL) Modular Ocean Model (MOM; version 2.2) and is described in detail in Weaver et al. (2001). The UVic ESCM has a global domain and model components share the same horizontal grid resolution. Control-state winds are prescribed by the 50-yr National Centers for Environmental Prediction reanalysis (NCEP-50) monthly mean climatology (Kistler et al. 2001). In all experiments, the ocean model has 19 vertical levels and the same vertical diffusivity profile. The Gent and McWilliams (1990, hereafter GM90) scheme is employed to parameterize the effects of unresolved mesoscale eddies. Resolution-dependent ocean bathymetry data are used, but the land mass and shape of the coastlines are both held fixed with increasing resolution by placing a minimum 125-m (ocean level 2) depth constraint on new bathymetry.

Four baseline models with horizontal resolutions of 1.8° × 3.6°, 0.6° × 1.2°, 0.3° × 0.6°, and 0.2° × 0.4° are equilibrated under year 1900 radiative forcing conditions. The higher-resolution models are initiated from the interpolated 3000-yr equilibrium state of the 1.8° × 3.6° model. Following the Reynolds grid number stability criterion of Bryan et al. (1975), the Laplacian horizontal mixing coefficient (A_M) for momentum is reduced by roughly the factor increase in resolution, as are the along-isopycnal (A_{ISO}) and isopycnal thickness diffusion (A_{ITH}) tracer mixing coefficients (Table 1). These baseline models are employed to investigate the resolution sensitivity of the Southern Ocean response to poleward intensifying winds from the years 1900 to 2100. Model drift is accounted for by differencing simulations forced with increasing atmospheric CO_2 concentration concomitant with Southern Hemisphere surface wind anomalies from those forced with increasing CO_2 alone. Hence, anomalies presented from this experiment (hereafter referred to as the RESWIND experiment) illustrate the direct effect of poleward intensifying winds on the Southern Ocean along with the influence of buoyancy feedbacks between the wind and CO_2 forcing. In these experiments CO_2 increases from 295 ppm in 1900 to 830 ppm by 2100. Monthly surface wind anomalies assembled from simulations performed by 10 different global climate models from the World Climate Research Programme (WCRP) Coupled Model Intercomparison Project (phase 3; CMIP3) multimodel ensemble (forced by the same CO_2 trajectory; see Fyfe et al. 2007) are added to the NCEP-50 climatology in the Southern

TABLE 1. Horizontal resolution parameters and salient Southern Ocean features of simulations. Here A_M, A_{ISO}, and A_{ITH} are the horizontal, isopycnal, and isopycnal thickness diffusion coefficients, respectively. Sea ice thickness is taken as the average south of 65°S. Sea ice volume is the total Southern Ocean volume. DPT refers to the volume transport through Drake Passage. Poleward shifts in ACC position are determined by calculating the mean position of the mean ACC transport in each basin. Anomalies presented for 1.8° × 3.6°, 0.6° × 1.2°, 0.3° × 0.6°, and the first column of 0.2° × 0.4° High A_M values are in response to RESWIND forcing. Anomalies presented at 0.2° × 0.4° Low A_M and the second column of 0.2° × 0.4° High A_M are in response to VISCWIND forcing. All values are determined from 5-yr averages.

Resolution	1.8° × 3.6°	0.6° × 1.2°	0.3° × 0.6°	0.2° × 0.4° High A_M	0.2° × 0.4° Low A_M
A_M (10^8 cm^2 s^{-1})	20	7	3	1.5	0.1
A_{ISO}, A_{ITH} (10^6 cm^2 s^{-1})	4	1.5	1	0.75	0.75
Equilibration (yr)	3000	450	100	50	20
Sea ice thickness (m)	0.46	0.57	0.71	0.67	0.62
Sea ice vol. (10^{12} m^3)	4.97	5.72	7.15	6.95	5.25
Sea ice vol. anomaly (10^{12} m^3)	−0.40	−0.38	−0.51	−0.64/−0.85	−1.01
DPT (Sv)	115	197	210	177	152
DPT anomaly (Sv)	11.1	14.2	10.5	14.7/22.2	9.0
Atlantic shift (°S)	1.63	1.81	1.85	2.70/1.86	1.87
Indian shift (°S)	2.50	0.99	1.15	1.98/2.53	3.41
Pacific shift (°S)	0.68	0.19	0.27	0.36/0.45	0.56
Global shift (°S)	1.47	0.88	1.01	1.41/1.35	1.85

Hemisphere only. Figure 1 shows the spatial distribution of wind stress anomalies averaged over the years 2095–2100. By 2100 the maximum zonal wind stress increases by about 25% and shifts poleward by roughly 3.5°.

In our baseline model with the highest resolution (0.2° × 0.4°) the zonal average near-surface Southern Ocean eddy kinetic energy is roughly one-tenth of observed values, a consequence of the large A_M value required to avoid erroneous computational modes (Spence et al. 2009). To make the dissipation more scale selective, one possibility is to employ the biharmonic form of lateral viscosity. However, this would require introducing different parameterizations for the different model resolutions—something we try to avoid in this intercomparison study. On the other hand, the applicability of the Bryan et al. (1975) linear criterion to coupled model solutions based on primitive equations is not entirely straightforward (e.g., Jochum et al. 2008). Therefore, in addition to our baseline simulations, we discuss a 0.2° × 0.4° simulation wherein the Laplacian viscosity coefficient is decreased to 0.1×10^8 cm^2 s^{-1}. This simulation was equilibrated for 20 years, starting from the final control state (year 50) of the 0.2° × 0.4° baseline model run. The decrease of the viscosity coefficient results in an increase of the zonal average near-surface Southern Ocean eddy kinetic energy to roughly one-fifth of observed values. In a second experiment (hereafter referred to as the VISCWIND experiment) we evaluate the viscosity sensitivity of the highest-resolution model response to the WCRP CMIP3 monthly surface wind anomalies. Both the baseline (hereafter referred to as 0.2° × 0.4° High A_M) and the lower viscosity 0.2° × 0.4° (hereafter 0.2° × 0.4° Low A_M) simulations are forced from their year 1900 control state exclusively with poleward intensifying winds anomalies over the years 2060 to 2100. Model drift is accounted for by differencing the forcing runs from control-state runs that were also integrated for an additional 40 years. We note that this experiment tests the direct effect of poleward intensifying winds on the Southern Ocean

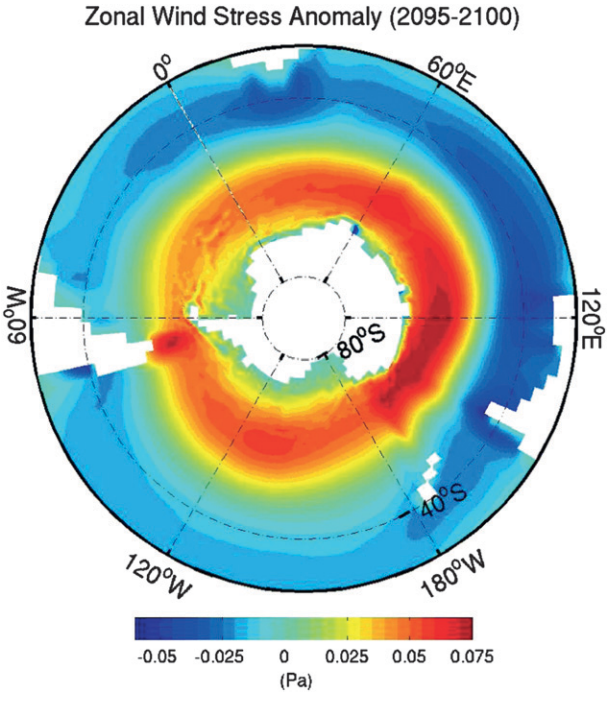

FIG. 1. Zonal surface wind stress anomaly averaged over years 2095–2100 Minor differences between simulations in the wind stress forcing at high latitudes can result from differences in sea ice drag (shown for the High A_M 0.2° × 0.4° model).

without the influence of buoyancy feedbacks between the wind and CO_2 forcing.

3. Results

The Southern Ocean temperature response to poleward intensifying winds can be characterized as having more regional structure and local intense anomalies at higher resolution. Figure 2a shows that at 1.8° × 3.6° the temperature response to the RESWIND forcing is relatively diffuse and zonally uniform, with warming between roughly 40° and 55°S and cooling at higher and lower latitudes. Much of the warming results from an increase in downward Ekman pumping that deepens isotherms, while a reduction in downward Ekman pumping north of roughly 40°S and an intensification of upward Ekman pumping south of about 60°S produces a shallowing of isotherms and cooling (Fyfe et al. 2007). This pattern of temperature response remains robust at higher resolution in both the RESWIND (Figs. 2b–d) and VISCWIND (Figs. 2e,f) experiments and is in general agreement with observed anomalies during positive SAM events (Ciasto and Thompson 2008). However, the higher-resolution models all exhibit intense local warming anomalies, particularly in the Atlantic where some exceed an average of 5.0°C over the upper 980 m. The higher-resolution models also have local regions of large cooling, particularly at midlatitudes in the Indian and Pacific basins. Overall, the RESWIND simulations demonstrate an increase in the local intensity and spatial variability of temperature response with resolution. The 0.2° × 0.4° VISCWIND simulations demonstrate a similar decline in zonal uniformity as horizontal viscosity is reduced.

The relatively strong Atlantic warming of the VISCWIND 0.2° × 0.4° High A_M simulation is an intriguing outlier of Fig. 2, particularly in comparison to this model's relatively weak response to RESWIND forcing. Differences between the RESWIND and VISCWIND response of this model (Figs. 2d,e) could be attributed to the different surface buoyancy forcing, internal variability, or different wind forcing. Figure 3 shows the ocean surface buoyancy fluxes for the 0.2° × 0.4° High A_M simulations, along with those of the NCEP 50-yr reanalysis model for a general comparison (Kistler et al. 2001). North of 65°S the NCEP reanalysis fluxes compare reasonably well with the 0.2° × 0.4° High A_M control state, and significant differences south of 65°S are not surprising given the NCEP reanalysis dependence on scarce high-latitude observations (especially in winter) and the exclusion of brine rejection. Figure 3 also shows that the flux anomalies in response to RESWIND and VISCWIND forcings are quite similar, making it unlikely that buoyancy forcing is responsible for the differences between Figs. 2d and 2e.

How much of the difference between simulations is due to internal variability is an important and challenging question. Recalculating Fig. 2 using time average periods of 2090–2095 and 2090–2100 reveals results quite similar to those shown for the 2095–2100 period. In fact, when all figures presented in this paper (except for Figs. 5e and 5f, which require computationally intensive snapshot data) were evaluated using these different time averaging periods, those presented herein for the 2095–2100 were found to be robust. While longer-term variability may be critically important, the evidence suggests that the difference between Figs. 2d and 2e results from the different wind forcing. In particular, we shall see that the intensity of warming is strongly affected by the shifting of temperature fronts in conjunction with the ACC.

Figure 2 includes the 2095–2100 mean ACC position determined for each simulation by adding forcing-induced anomalies to the control-state ACC position. All simulations show poleward migration of the ACC in the Atlantic and the western half of the Indian basin, while only slight changes are found in the eastern Indian and Pacific basins. Note that the large region of strong wind stress anomalies south of Australia (Fig. 1) does not drive a significant shift in the ACC position, which highlights the importance of bathymetry in guiding the ACC path in this region. Table 1 shows that when averaged globally and over individual basins all the 0.2° × 0.4° simulations exhibit shifts in ACC position comparable to the coarser-resolution models, supporting observational evidence that a southward displacement of the ACC can occur along with the effects of enhanced mesoscale eddies on transport (Böning et al. 2008). The observational analysis of Gille (2008) indicates that the long-term Southern Ocean temperature trend is regionally consistent with a poleward displacement of temperature fronts in conjunction with the ACC, and that the shifting of fronts could account for nearly 90% of the observed warming.

We evaluate Southern Ocean fronts from 5-yr averages of meridional temperature gradients at 285-m depth, following the Belkin and Gordon (1996) definition of the Subantarctic Front. Southern Ocean temperature fronts are observed as complex, zonal branches or filaments with meridional gradients often exceeding 0.04°C km^{-1} (e.g., Plate 1c of Hughes and Ashe 2001; Fig. 5b of Sallee et al. 2008). We find that increasing model resolution strongly enhances the ability to resolve the spatial complexity and intensity of Southern Ocean fronts. At 1.8° × 3.6° the control-state meridional temperature gradients are very diffuse and weak in comparison to observations, with maximum intensities below 0.025°C km^{-1} (not shown). The intensity of fronts is improved at 0.3° × 0.6° and 0.6° × 1.2°, but spatially they are characterized by

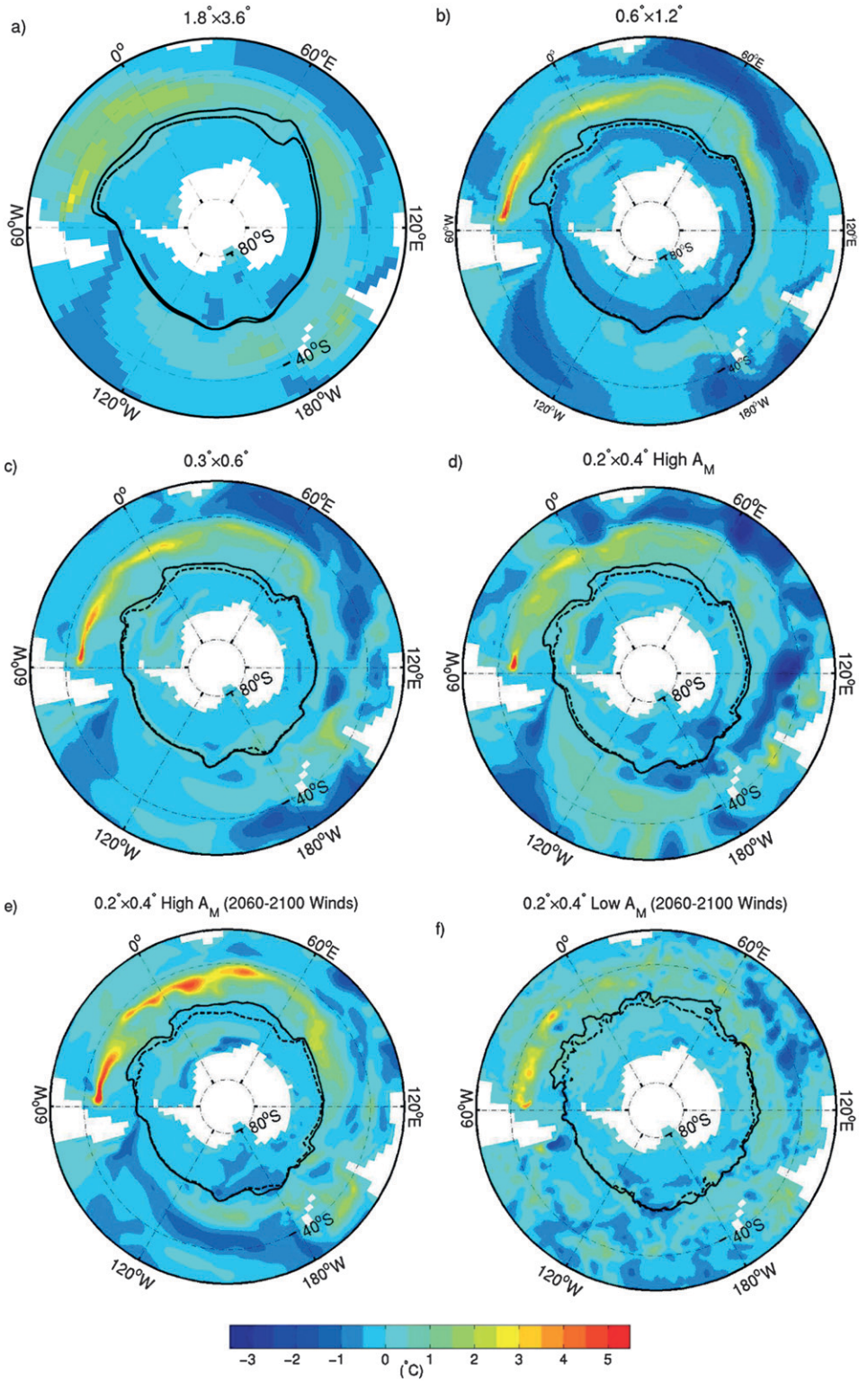

FIG. 2. Ocean temperature anomaly (°C) averaged over the upper 980 m and years 2095–2100 (color). Position of mean ACC transport in the 5-yr control-state average (solid black line) and over 2095–2100 (dashed black line). (a)–(d) Response of the four baseline models to RESWIND forcing (1900–2100). (e),(f) Response of the high– and low–horizontal viscosity (A_M) 0.2° × 0.4° simulations to VISCWIND forcing (2060–2100).

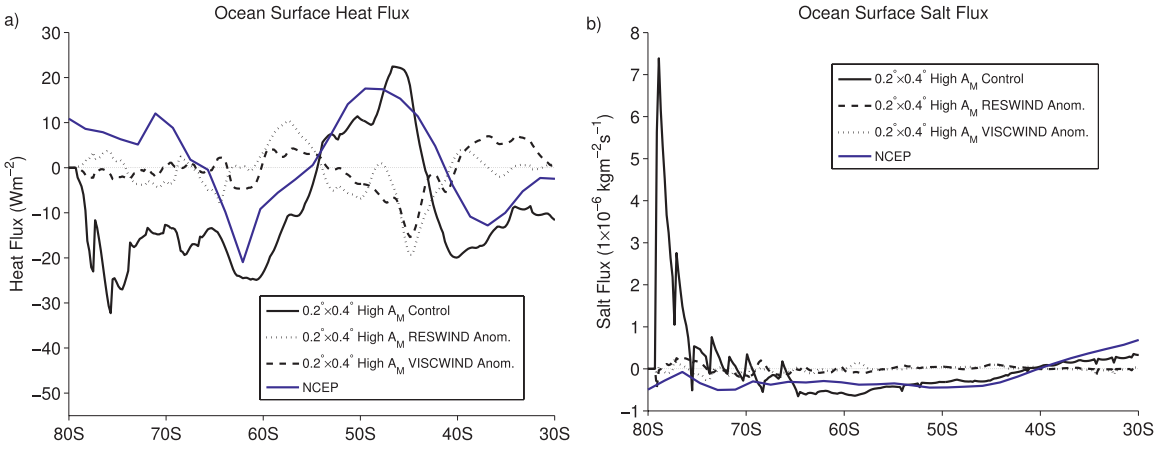

FIG. 3. Zonal average (a) surface heat and (b) salt flux into the ocean (positive downward). Five-yr control-state average of the 0.2° × 0.4° High A_M simulation (solid black), annual mean of NCEP 50-yr reanalysis (solid blue), and average anomaly over years 2095–2100 in the RESWIND (dashed) and VISCWIND (dotted) simulation of 0.2° × 0.4° High A_M (dashed black).

zonal bands that are too extensive compared to observations (not shown). Figures 4a and 4b show that both the High A_M and Low A_M 0.2° × 0.4° simulations present reasonable comparisons to observations in terms of the intensity and spatial distribution of fronts. While fronts in the 0.2° × 0.4° High A_M simulation tend to lack complexity and be too zonally extensive, and the 0.2° × 0.4° Low A_M simulation is too diffuse, they both offer significant improvements over the coarser-resolution models. The improvement likely results both from the effects of increasing the resolution of bathymetry, which acts to guide the position of fronts, and from the ability to resolve smaller-scale structures at higher resolution.

Figures 4c and 4d present meridional temperature gradient anomalies from the 0.2° × 0.4° High A_M and Low A_M simulations in response to the VISCWIND forcing. We note that the strong anomaly dipole patterns found in the Atlantic and Indian basins, particularly in the High A_M simulation, are indicative of a southward shift in frontal positions. This is in general agreement with available hydrographic observations, which find a poleward movement of fronts in the Indian basin, an equatorward movement in the central Pacific, and a little meridional movement in the Indo-Pacific basin during positive SAM events (Sallee et al. 2008). A comparison between Figs. 2e,f and 4c,d reveals that locations of intense warming are collocated with poleward shifts in temperature fronts and ACC position. In fact, all warming signals >2.5°C found in Fig. 2 are associated with the southward migration of temperature fronts, in agreement with the hypothesis of Gille (2008). Furthermore, the weaker Atlantic warming response of the 0.2° × 0.4° High A_M model to RESWIND forcing in comparison to VISCWIND forcing (Figs. 2d,e) can be largely attributed to weaker frontal shifts. Given that the different frontal shifts of the 0.2° × 0.4° High A_M simulations could not be definitively attributed to internal variability or buoyancy forcing (discussed above), this points to the powerful but somewhat fickle nature of frontal displacements to wind forcing.

Figures 3a and 3b show that in a zonal and depth-averaged view the general structure of the temperature response to both RESWIND (Fig. 5a) and VISCWIND forcing (Fig. 5b), with warming between roughly 40° and 55°S and cooling at higher and lower latitudes, is robustly produced in all the simulations. We note that the greater low- and high-latitude cooling found in the RESWIND experiment at 0.6° × 1.2° is due to Ekman upwelling of colder subsurface waters found in this simulation. We also note that the distinct peaks of amplified warming found at 43°S in the 0.3° × 0.6° RESWIND simulation and both the RESWIND and VISCWIND 0.2° × 0.4° High A_M simulations illustrate the strong effect of meridional shifts in temperature fronts. A reduction in zonal mean cooling (particularly between roughly 55° and 65°S) is found in the two higher-resolution models of the RESWIND experiment relative to the coarse-resolution models, as well as in the 0.2° × 0.4° Low A_M response to VISCWIND forcing relative to the High A_M simulation.

Table 1 shows that despite all models having a zonal mean cooling response south of 55°S to the wind forcing scenarios, each also exhibits a significant reduction in sea ice volume. This is primarily due to an increased wind-driven transport of sea ice equatorward into warmer waters. We do note a tendency toward a greater decline in sea ice volume as mesoscale activity is better resolved. The average percent reduction of sea ice volume among the four models of the RESWIND experiment is 7.7%, with the 0.2° × 0.4° High A_M simulation showing the

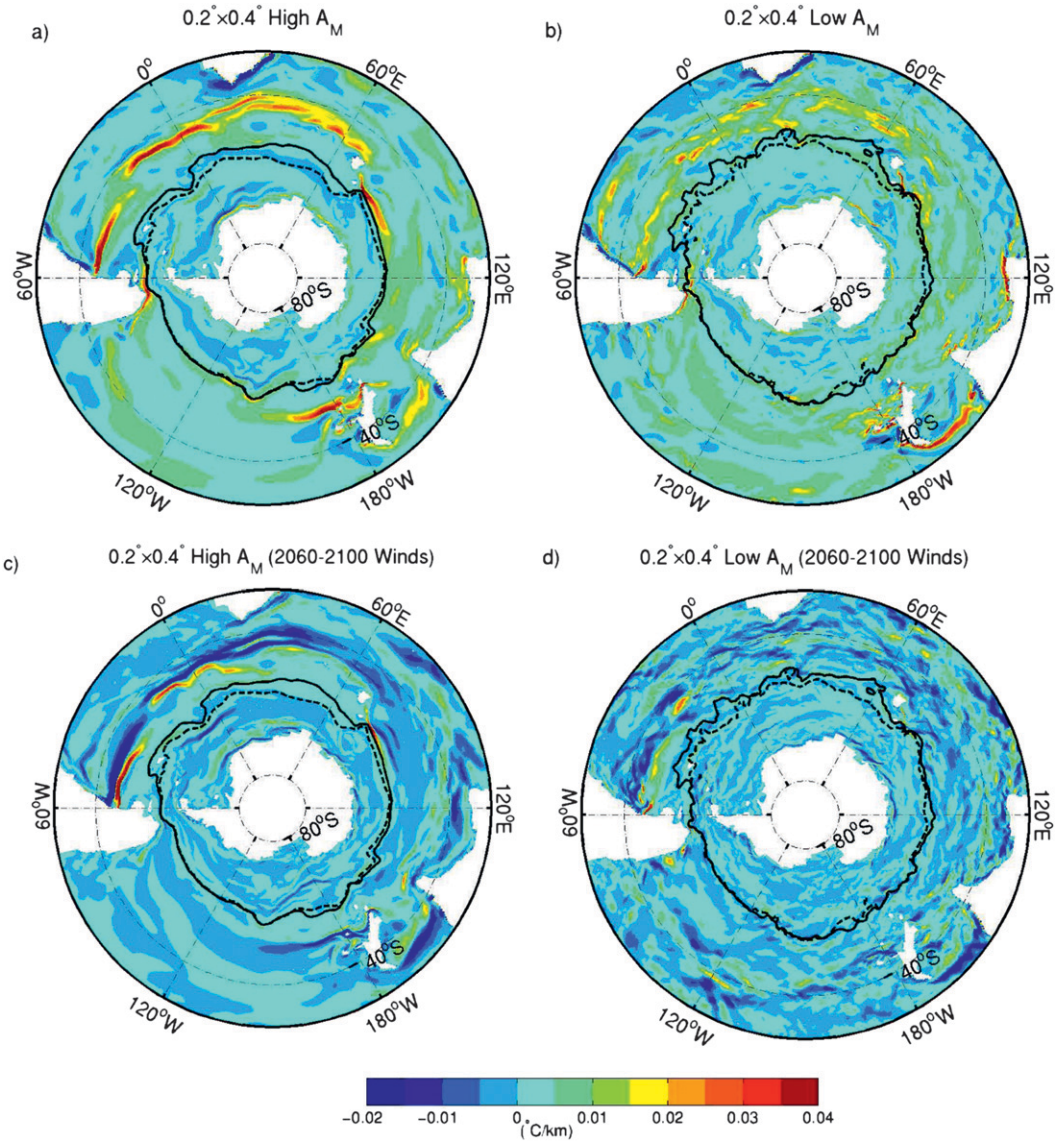

FIG. 4. Meridional temperature gradients (°C km^{-1}; color) in the high– and low–horizontal viscosity 0.2° × 0.4° simulations at 285-m depth. (a),(b) Five-yr control-state averages and (c),(d) gradient anomalies from VISCWIND forcing averaged over years 2095–2100. ACC position (black lines) plotted as in Fig. 2.

largest loss (9.2%). In the VISCWIND experiment the percent reduction of sea ice volume is increased to 12.2% and 19.2% for the 0.2° × 0.4° High A_M and Low A_M simulations, respectively. The average Southern Ocean sea ice thickness in the control states of the simulations (Table 1) compares well to the 0.62-m observational estimate of Worby et al. (2008). Figures 5c and 5d show the zonal average sea ice thickness anomalies for the RESWIND and VISCWIND experiments, respectively. The 1.8° × 3.6° to 0.3° × 0.6° models all have similar reductions in ice thickness, but there is a substantial increase in the amplitude and spatial variability of anomalies at 0.2° × 0.4° in both the RESWIND and VISCWIND experiments, which is largely due to enhanced sea ice dynamics near the Antarctic Peninsula. While all models show a significant loss of ice on the east coast (or downwind side) and a slight gain on the west coast (or upwind side) of the Antarctic Peninsula, this effect is strongly amplified in the 0.2° × 0.4° simulations (Fig. 6) as the winds pile substantially more ice on the upwind side (around 70°S) and drive offshore more ice on the downwind side. It should be noted that recent satellite observations of sea ice reveal a differing trend, one of ice loss (gain) on the west (east) side of the Antarctic Peninsula (Comiso and Nishio 2008), which is not surprising given that anthropogenic surface heat

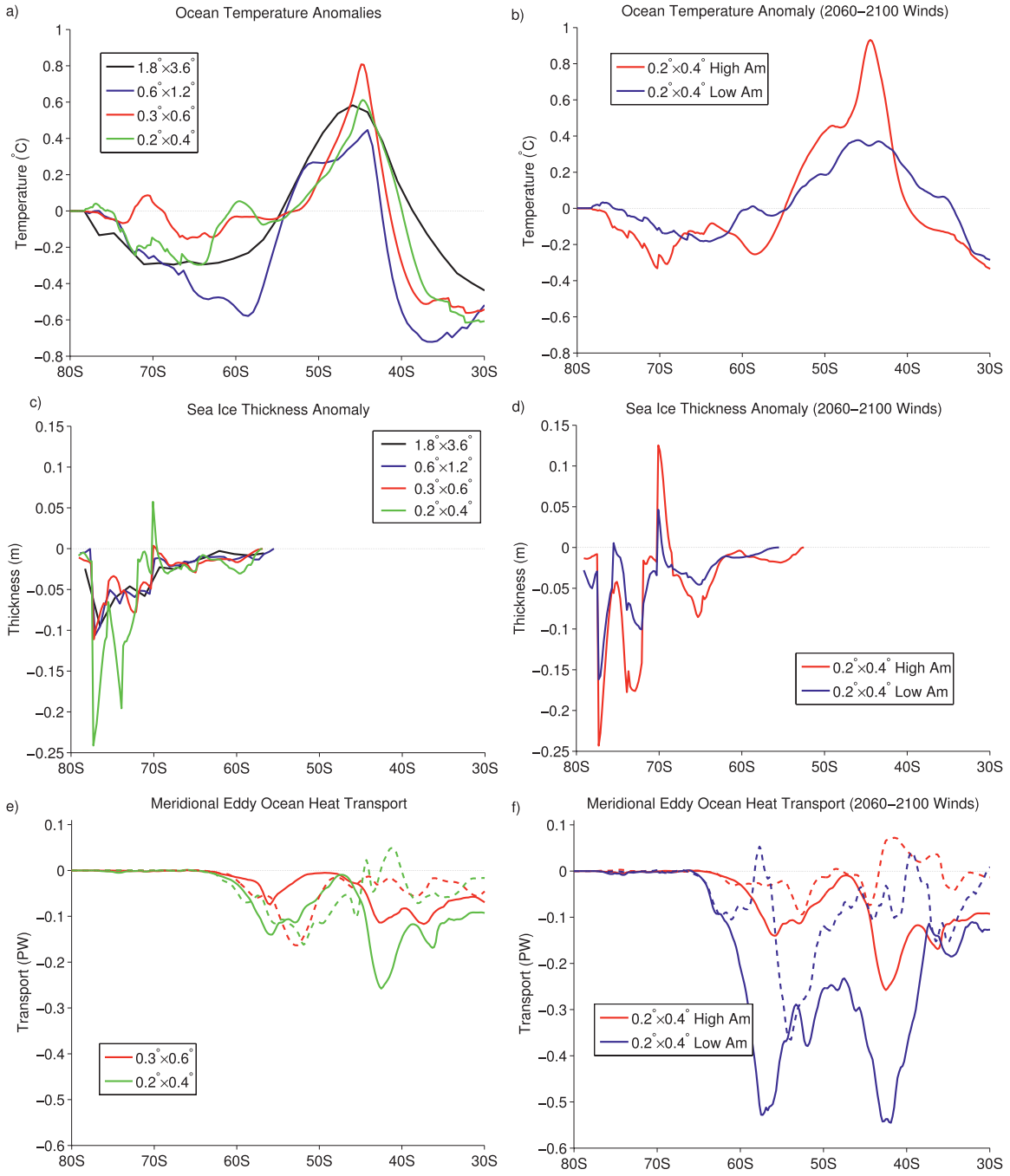

FIG. 5. (a),(b) Zonal average of ocean temperature anomalies from Fig. 2. (c),(d) Change in zonal average sea ice thickness averaged over years 2095–2100. (e),(f) Zonal and depth-integrated meridional ocean resolved eddy heat transport in control states (lines) and year 2100 anomalies (dashes) for the eddy-permitting models. (a),(c),(e) Results from the four baseline simulations to RESWIND forcing (1900–2100). (b),(d),(f) Results from the High and Low A_M 0.2° × 0.4° simulations to VISCWIND forcing (2060–2100).

flux forcing is largely ignored here (Comiso and Nishio 2008).

Figures 5e and 5f show the zonal and depth-integrated resolved eddy meridional heat transport in the control states of the 0.3° × 0.6° and 0.2° × 0.4° High A_M (plotted in both Figs. 5e and 5f) and 0.2° × 0.4° Low A_M simulations. The transports are calculated as $\overline{\mathbf{v}'\theta'} = \overline{\mathbf{v}\theta} - \overline{\mathbf{v}}\,\overline{\theta}$ (primed values refer to the eddy components and the overbar denotes temporal averaging), from instantaneous snapshots of meridional velocity ($\mathbf{v}$) and potential temperature (θ) recorded at 5-day intervals for 1 year. As pointed out by McIntosh and McDougall (1996),

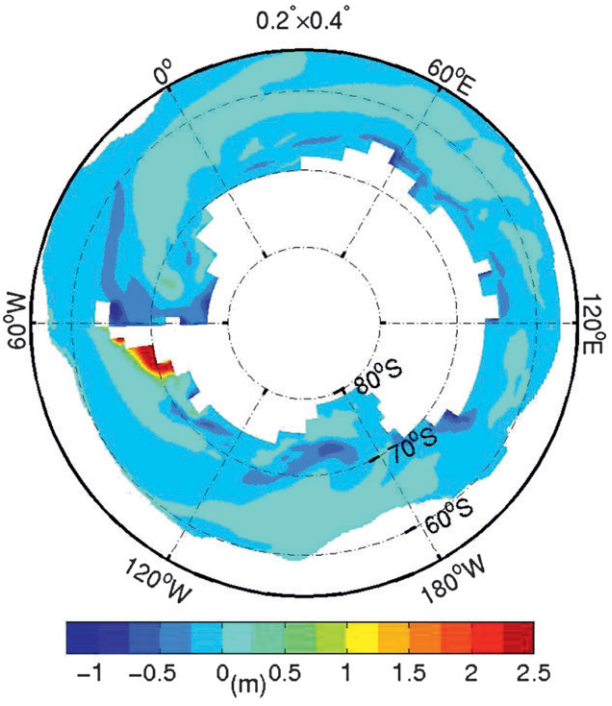

FIG. 6. Sea ice thickness anomaly of 0.2° × 0.4° High A_M in response to VISCWIND forcing (2060–2100).

in a model where there is no explicit interannual forcing, such as ours, using several years of snapshots instead of one year should not result in substantial changes in this type of calculation. Southern Ocean eddy heat flux estimates from observations suggest a southward cross-ACC flux ranging between 0.3 and 0.9 PW (Gille 2003), which is the same order of magnitude as the observed time mean heat transport (Macdonald and Wunsch 1996). All of our high-resolution simulations exhibit a net southward Southern Ocean eddy heat transport with the largest contributions found near topographic features, particularly the Crozet Plateau (near 43°S) and the Kerguelen and Campbell Plateaus (both near 55°S). Both the 0.3° × 0.6° and 0.2° × 0.4° High A_M control-state eddy heat transports are below observed estimates, but they compare well with the 0.25° × 0.25° model of Jayne and Marotzke (2002). The 0.2° × 0.4° Low A_M simulation produces Southern Ocean eddy heat transports well within the range of observations. Note that the GM90-induced Southern Ocean heat transport in these high-resolution models, as well as the resolved eddy heat transport of the coarser-resolution models, is relatively insignificant (i.e., zonal means less than 0.025 PW; not shown).

Figures 5e and 5f also show the year 2100 meridional eddy heat transport anomalies of the high-resolution models in response to RESWIND and VISCWIND forcing, respectively. Resolved eddies in all the high-resolution simulations exhibit a significant net increase in southward transport between 45° and 65°S that can account for some of the reduced cooling found between 55° and 65°S found at eddy-permitting resolutions. In particular, the 0.2° × 0.4° Low A_M simulation shows an average increase of 0.13 PW between 50° and 65°S, which is roughly 45% of the model's control-state resolved eddy heat transport. Note that the GM90 parameterization induces negligible change in heat transport in response to the wind forcing in the coarse-resolution models (not shown).

Sea surface height and bottom pressure observations since the early 1980s show that ACC transport is positively correlated with interannual SAM variability (Hughes et al. 2003; Meredith et al. 2004). However, the study of Böning et al. (2008) finds no discernible increase in the tilt of isopycnal surfaces in observational data over the past four decades, implying that the ACC transport is insensitive to wind stress changes on decadal time scales, a result supporting eddy-resolving model studies (Hallberg and Gnanadesikan 2006; Meredith and Hogg 2006; Screen et al. 2009). However, poleward intensifying wind forcing is expected to amplify through the next century, and while the atmospheric signal is clearly discernible from observations, it is currently weak compared to expected changes. The ACC has the largest volume transport in the global ocean, with an estimated transport through the Drake Passage of roughly 135 Sv (1 Sv $\equiv 10^6$ m^3 s^{-1}; Cunningham et al. 2003), and changes in its transport may be of substantial importance to the earth's climate in the future (Zickfeld et al. 2007).

Table 1 shows that our control simulations have Drake Passage transports ranging from 115 to 210 Sv. The mismatch between observed and modeled values is not surprising, as only 3 of 18 WCRP CMIP3 models produce transports within 20% of the highly uncertain observations (Russell et al. 2006). Figures 7a–c show that Drake Passage transport is found to generally increase as the westerly winds intensify and shift poleward in all of the RESWIND simulations. Importantly, as the resolution increases so too does the interannual and longer time scale variability, which then acts to obscure the long-term anthropogenic effect of the poleward intensifying winds. For example, Fig. 7c shows no discernible anthropogenic change in the transport over the twentieth century, which is consistent with recent observations of ACC transport (Böning et al. 2008). However, we note that interpretations of variability in the time series of Figs. 7a–c are complicated by the fact that data points are calculated by differencing forced and control simulations at 5-yr intervals, and large anomalies can result if the variabilities of the two simulations are out of phase.

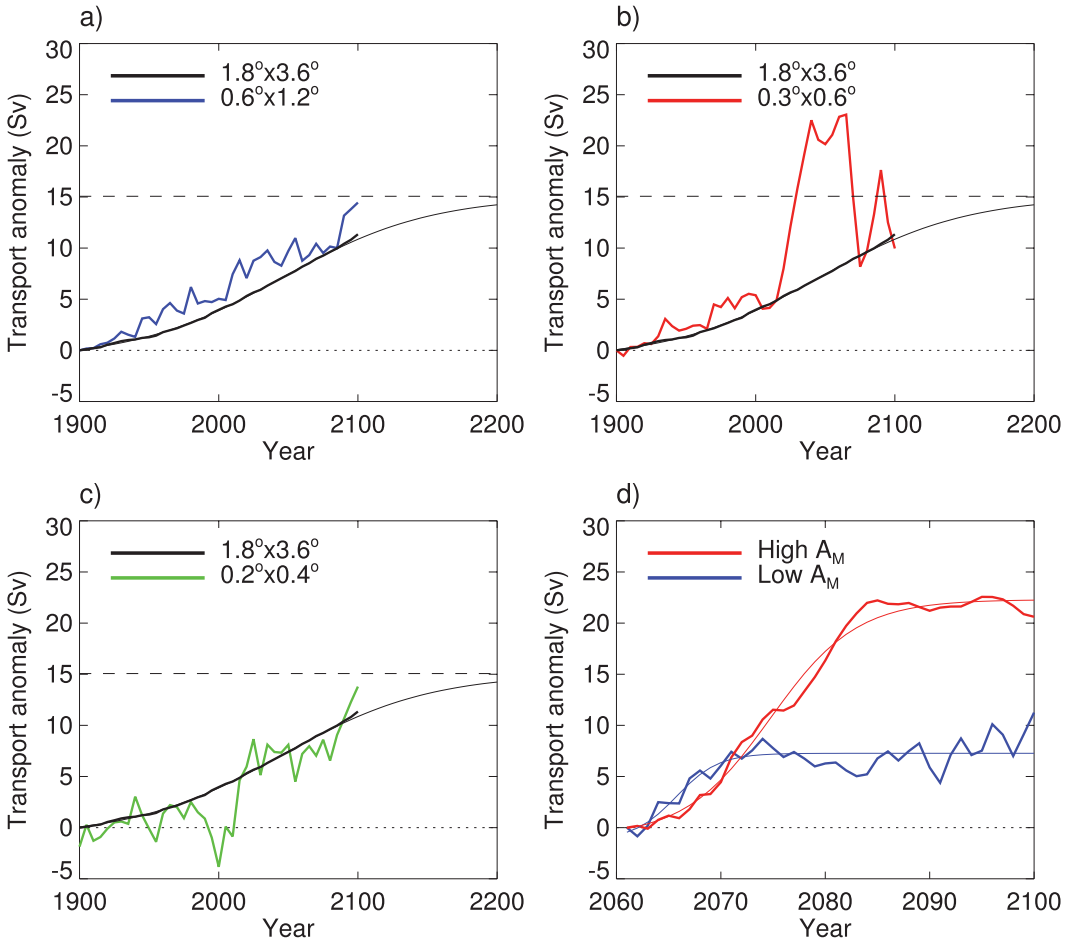

FIG. 7. (a)–(c) Change in the annual-mean Drake Passage transport (5-yr intervals) for RESWIND simulations. (d) Change in the annual-mean Drake Passage transport (1-yr intervals) for VISCWIND simulations.

For example, the anomaly variability in the latter portion of the twenty-first century at 0.3° × 0.6° (Fig. 7b) far exceeds that found in the transport time series of both the control of forcing simulations and results from the two time series being out of phase.

Figure 7d shows the Drake Passage transport anomalies for the VISCWIND experiment. Note that these anomalies are determined by differencing forced and control simulations at 1-yr intervals, and consequently they tend to show less variability than the high-resolution models of the RESWIND experiment. The Drake Passage transport response of the 0.2° × 0.4° High A_M simulation follows an approximately inverse tangent profile, increasing over the first 20 yr and then stabilizing. Figure 8a shows that the net 22-Sv increase in transport for this simulation correlates with a substantial deepening and steepening of Southern Ocean isopycnals. On the other hand, Figs. 7d and 8b show that the 0.2° × 0.4° Low A_M exhibits a comparatively modest 9-Sv increase in transport over the first decade and then stabilizes, with little change in the slope and depth of isopycnals. The weaker transport and isopycnal response of the 0.2° × 0.4° Low A_M simulation indicates that the effect of wind stress forcing on ACC transport in models is dependent on the representation of mesoscale eddy activity, in agreement with Southern Ocean eddy-resolving model results (e.g., Hallberg and Gnanadesikan 2006; Meredith and Hogg 2006; Screen et al. 2009). It implies that poleward intensifying wind stress forcing may have a small effect on the real ACC transport on decadal time scales, corroborating results discerned from observational data (Böning et al. 2008). However, we note that the increase in transport variability found as eddy activity is better resolved (see Fig. 7d) demonstrates the need for study over relatively long time periods.

4. Conclusions

Versions of the same global climate model, ranging in horizontal resolution from 1.8° × 3.6° to 0.2° × 0.4°, are

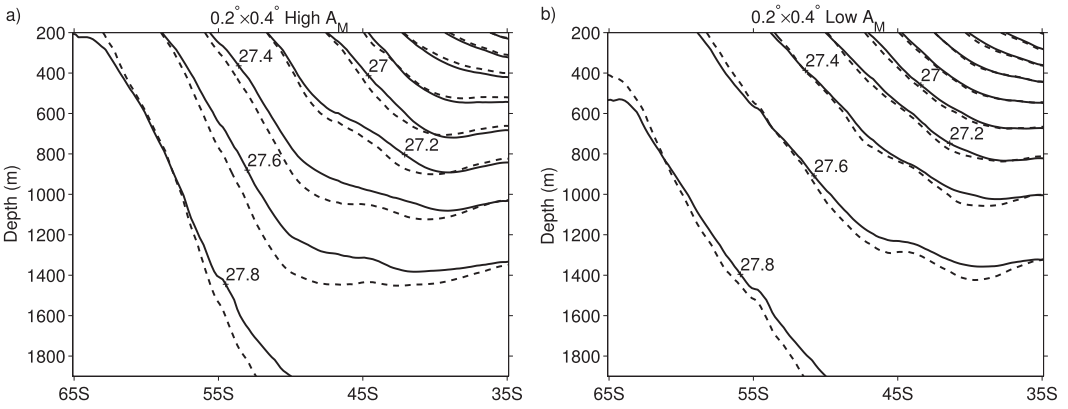

FIG. 8. Zonal average isopycnals in the High and Low A_M 0.2° × 0.4° simulations. Five-yr control-state average (solid) and 2095–2100 average position (dashes) in response to VISCWIND forcing (2060–2100). Plotted as sigma potential density referenced to the surface (0.2 kg m^{-3} contours).

employed to investigate the resolution dependence of the Southern Ocean response to poleward intensifying winds through the twenty-first century. It is found that the zonal mean structure of the Southern Ocean temperature response, with warming between 40° and 55°S and cooling at higher and lower latitudes, remains robust as model resolution increases and mesoscale activity is better resolved. However, as expected, the response to wind anomalies has more regional structure at higher resolution. This is particularly evident in the warming of the Atlantic and Indian basins, where the southward migration of better-resolved ocean temperature fronts can produce a strong (i.e., >2.5°C when averaged over the upper 980 m) localized warming, in agreement with the observations of Gille (2008). Parameterized eddy heat transport, required at coarse resolutions, is relatively insensitive to the wind forcing, while resolved eddies at higher resolutions can exhibit a significant (i.e., up to 45%) increase in southward heat transport. As mesoscale activity is better resolved there is also a reduction in the zonal mean cooling response south of about 55°S, and a greater loss of sea ice volume. Together the high-resolution simulations show a 9%–19% (dependent on forcing scenario and model configuration) reduction in Southern Ocean sea ice volume.

A southward migration of the ACC is found in response to poleward intensifying winds irrespective of the degree of resolved mesoscale activity. Together, the simulations suggest a global mean ACC shift of roughly 1.3°S, an Atlantic and Indian Ocean mean shift of 2.0°S, and a Pacific Ocean mean shift of 0.4°S within this century. ACC volume transport is found to initially increase with enhanced westerly wind stress forcing in all of the simulations. However, as mesoscale activity is better resolved the transport anomaly tends to stabilize after an initial period of increase. This implies that the affect of wind stress forcing on ACC transport in models is dependent on the resolution of mesoscale eddy activity on decadal time scales, in agreement with eddy-resolving model results (e.g., Hallberg and Gnanadesikan 2006; Meredith and Hogg 2006; Screen et al. 2009) and recent observational data (Böning et al. 2008).

Acknowledgments. We wish to thank Oleg Saenko and Matthew England for their insightful comments. This research was supported by the NSERC/CFCAS CLIVAR program. Infrastructure support from CFI, NEC, BCKDF, UVic, and UNSW is also acknowledged. We are also very grateful to the anonymous referees.

REFERENCES

Aoki, S., M. Yoritaka, and A. Masuyama, 2003: Multidecadal warming of subsurface temperature in the Indian sector of the Southern Ocean. *J. Geophys. Res.,* **108,** 8081, doi:10.1029/2000JC000307.

Belkin, I., and A. Gordon, 1996: Southern Ocean fronts from the Greenwich meridian to Tasmania. *J. Geophys. Res.,* **101,** 3675–3696.

Böning, C., A. Dispert, M. Visbeck, S. Rintoul, and F. Scharzkopf, 2008: The response of the Antarctic Circumpolar Current to recent climate change. *Nat. Geosci.,* **1,** 864–869.

Bryan, K., S. Manabe, and C. Pacanowski, 1975: A global ocean–atmosphere climate model. Part II: The oceanic circulation. *J. Phys. Oceanogr.,* **5,** 30–46.

Ciasto, L., and D. Thompson, 2008: Observations of large-scale ocean–atmosphere interaction in the Southern Hemisphere. *J. Climate,* **21,** 1244–1259.

Comiso, J., and F. Nishio, 2008: Trends in the sea ice cover using enhanced and compatible AMSR-E, SSM/I, and SMMR data. *J. Geophys. Res.,* **113,** C02S07, doi:10.1029/2007JC004257.

Cunningham, S., S. Alderson, B. King, and M. A. Brandon, 2003: Transport and variability of the Antarctic Circumpolar Current

in Drake Passage. *J. Geophys. Res.,* **108,** 8084, doi:10.1029/2001JC001147.

Fyfe, J., 2006: Southern Ocean warming due to human influence. *Geophys. Res. Lett.,* **33,** L19701, doi:10.1029/2006GL027247.

——, and O. Saenko, 2006: Simulated changes in the extratropical Southern Hemisphere winds and currents. *Geophys. Res. Lett.,* **33,** L06701, doi:10.1029/2005GL025332.

——, ——, K. Zickfeld, M. Eby, and A. Weaver, 2007: The role of poleward-intensifying winds on Southern Ocean warming. *J. Climate,* **20,** 5391–5400.

Gent, P., and J. McWilliams, 1990: Isopycnal mixing in ocean circulation models. *J. Phys. Oceanogr.,* **20,** 150–155.

Gille, S., 2002: Warming of the Southern Ocean since the 1950s. *Science,* **295,** 1275–1277.

——, 2003: Float observations of the Southern Ocean. Part II: Eddy fluxes. *J. Phys. Oceanogr.,* **33,** 1182–1196.

——, 2008: Decadal-scale temperature trends in the Southern Hemisphere ocean. *J. Climate,* **21,** 4749–4765.

Gillett, N., and D. Thompson, 2003: Simulation of recent Southern Hemisphere climate change. *Science,* **302,** 273–275.

Hallberg, R., and A. Gnanadesikan, 2001: An exploration of the role of transient eddies in determining the transport of a zonally reentrant current. *J. Phys. Oceanogr.,* **31,** 3312–3330.

——, and ——, 2006: The role of eddies in determining the structure and response of the wind-driven Southern Hemisphere overturning: Results from the Modeling Eddies in the Southern Ocean (MESO) project. *J. Phys. Oceanogr.,* **36,** 2232–2252.

Hogg, A., M. Meredith, J. Blundell, and C. Wilson, 2008: Eddy heat flux in the Southern Ocean: Response to variable wind forcing. *J. Climate,* **21,** 608–620.

Hughes, C., and E. Ashe, 2001: Eddy forcing of the mean flow in the Southern Ocean. *J. Geophys. Res.,* **106,** 2713–2722.

——, P. Woodworth, M. Meredith, and V. Stepanov, 2003: Coherence of Antarctic sea levels, Southern Hemisphere Annular Mode, and flow through Drake Passage. *Geophys. Res. Lett.,* **30,** 1464, doi:10.1029/2003GL017240.

Jayne, S., and J. Marotzke, 2002: The oceanic eddy heat transport. *J. Phys. Oceanogr.,* **32,** 3328–3345.

Jochum, M., G. Danabasoglu, M. Holland, Y. Kwon, and W. Large, 2008: Ocean viscosity and climate. *J. Geophys. Res.,* **113,** C06017, doi:10.1029/2007JC004515.

Kistler, R., and Coauthors, 2001: The NCEP–NCAR 50-Year Reanalysis: Monthly means CD-ROM and documentation. *Bull. Amer. Meteor. Soc.,* **82,** 247–267.

Macdonald, A., and C. Wunsch, 1996: An estimate of global ocean circulation and heat fluxes. *Nature,* **382,** 436–439.

McIntosh, P. C., and T. J. McDougall, 1996: Isopycnal averaging and the residual mean circulation. *J. Phys. Oceanogr.,* **26,** 1655–1660.

Meredith, M., and A. Hogg, 2006: Circumpolar response of Southern Ocean eddy activity to a change in the Southern Annular Mode. *Geophys. Res. Lett.,* **33,** L16608, doi:10.1029/2006GL026499.

——, P. Woodworth, C. Hughes, and V. Stepanov, 2004: Changes in the ocean transport through Drake Passage during the 1980s and 1990s, forced by changes in the Southern Annular Mode. *Geophys. Res. Lett.,* **31,** L21305, doi:10.1029/2004GL021169.

Russell, J., R. Stouffer, and K. Dixon, 2006: Intercomparison of the Southern Ocean circulations in IPCC coupled model control simulations. *J. Climate,* **19,** 4560–4575.

Sallee, J., K. Speer, and R. Morrow, 2008: Response of the Antarctic Circumpolar Current to atmospheric variability. *J. Climate,* **21,** 3020–3039.

Screen, J., N. Gillett, D. Stevens, G. Marshall, and H. Roscoe, 2009: The role of eddies in the Southern Ocean temperature response to the Southern Annular Mode. *J. Climate,* **22,** 806–818.

Sen Gupta, A., and M. England, 2006: Coupled ocean–atmosphere–ice response to variations in the Southern Annular Mode. *J. Climate,* **19,** 4457–4486.

Spence, P., O. Saenko, M. Eby, and A. Weaver, 2009: The Southern Ocean overturning: Parameterized versus permitted eddies. *J. Phys. Oceanogr.,* **39,** 1634–1651.

Thompson, D., and S. Solomon, 2002: Interpretation of recent Southern Hemisphere climate change. *Science,* **296,** 895–899.

Weaver, A. J., and Coauthors, 2001: The UVic Earth System Climate Model: Model description, climatology, and applications to past, present and future climates. *Atmos.–Ocean,* **39,** 361–428.

Worby, A., C. Geiger, M. Paget, M. Van Woert, S. Ackley, and T. DeLiberty, 2008: Thickness distribution of Antarctic sea ice. *J. Geophys. Res.,* **113,** C05S92, doi:10.1029/2007JC004254.

Zickfeld, K., J. Fyfe, O. Saenko, M. Eby, and A. Weaver, 2007: Response of the global carbon cycle to human-induced changes in Southern Hemisphere winds. *Geophys. Res. Lett.,* **34,** L12712, doi:10.1029/2006GL028797.